7870	200	0.3	1798	293	
A ($\sigma_{y,cs}$) (MPa)	B (MPa)	n	c	$\dot{\varepsilon}_0$ (s^{-1})	m
333	737	0.15	0.008	1	1.46

오류! 참조 원본을 찾을 수 없습니다. presents (a) the kinetic energy of the numerical model during impact loading, normalized by the initial kinetic energy for each velocity case, (b) the von Mises stress at the trailing edge of the foil profile of the blade at the fixed end, normalized by the yield stress at quasi-static strain rate of AISI 1020 carbon steel ($\sigma_{y,cs}$), with respect time, (c) the normal stress at z-direction (σ_{zz}), normalized by the yield stress at quasi-static strain rate of the material, with respect the corresponding normal strain (ε_{zz}), and (d) the equivalent plastic strain (ε_q) for both materials with respect the different velocities of the sea animal.

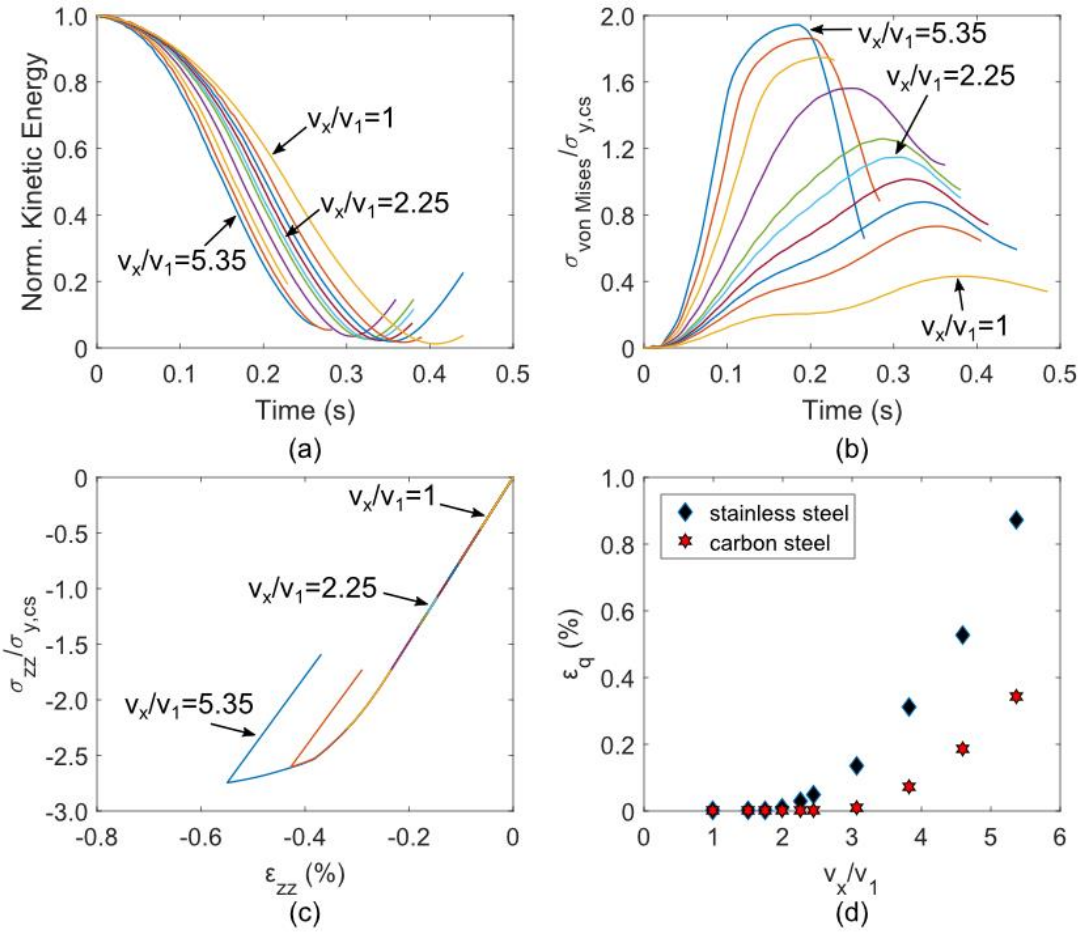

Figure 6. a) Normalized kinetic energy with respect time, b) normalized von Mises stress with respect time at the trailing edge of the foil profile at fixed end, c) normalized mormal stress at z-direction with respect the strain at the trailing edge of the foil profile at fixed end, d) equivalent plastic strain, for the different velocities of the killer whale; AISI 1020 carbon steel material.

The kinetic energy of the model for each velocity case follows the trend discussed in Section *3.1* accounting for stainless steel material. The kinetic energy drops during impact, while the deflection of the blade increases, reaching a minimum point when the maximum deflection occurs. The maximum deflection corresponds to the maximum von Mises stress at the trailing edge of the profile at the fixed end of the blade, while after that point the von Mises stress drops and the kinetic energy starts to increase, indicating push-back of the killer whale by the blade. Furthermore, it is shown that higher velocity of the sea animal is required to deform plastically the carbon steel material of the blade. Plastic deformation of the carbon steel material initiates at normalized velocity equal to 3.05, instead of 2.00 for the stainless steel material. In addition, the equivalent plastic strain of the blade made of carbon steel material is 87% lower than the blade with stainless steel material, considering the highest normalized velocity examined in the present work. However, the equivalent plastic strain for the case of stainless steel material is still low. The value is lower than 1%, even for velocity which corresponds to five times higher kinetic energy than the operational conditions assumed in the present study.

3.3 Multiple impacts

In the following, the dynamic response and the accumulation of the plastic strain in the blade's stainless steel material was simulated, considering multiple impacts. This is the first approach to investigate the influence of multiple impact events on the accumulation of plastic strain, which could lead to damaging of the material's microstructure, crack initiation, crack propagation and failure eventually of the turbine blade. For the analyses presented in the present section, the normalized velocity of the killer whale was assumed to be 3.05; this velocity corresponds to plastic strain approximately equal to 0.2%, which corresponds to the 0.2% offset yield point. Furthermore, it was imposed in each impact, the plastic strain of the turbine blade's stainless steel material simulated in the previous impact event, as initial condition, while ten impact events were simulated in total.

Figure *7* presents the compression at the trailing edge of the foil profile at the fixed end of the turbine blade. The normalized normal stress at z-direction ($\sigma_{zz}/\sigma_{y,ss}$) is shown for the increasing number of impact events, with respect the corresponding normal strain (ε_{zz}), while the arrow indicates the increasing number of impacts. The plastic deformation and the corresponding hardening of the stainless steel material leads to increasing the gradually the yield stress of the material. Therefore, the elastic energy which is required to reach the yield point increases, resulting in reducing the energy which corresponds to plastic deformation of the material; the initial energy is similar in every number of impact and corresponds to the initial kinetic energy. Furthermore, the equivalent plastic strain of the stainless steel material is also shown in Figure *8*, with respect the number of impacts. The figure shows that increasing the number of impacts the material hardens and the corresponding increase rate of the plastic strain decreases. Therefore, increasing the number of impacts and the corresponding hardening of the turbine blade's material, the velocity of the sea animal and the corresponding initial kinetic energy will result in elastic

deformation of the blade exclusively. This is an important correlation between the number of impacts required to result in elastic deformation of the material and the initial kinetic energy and it constitutes an open issue for future study.

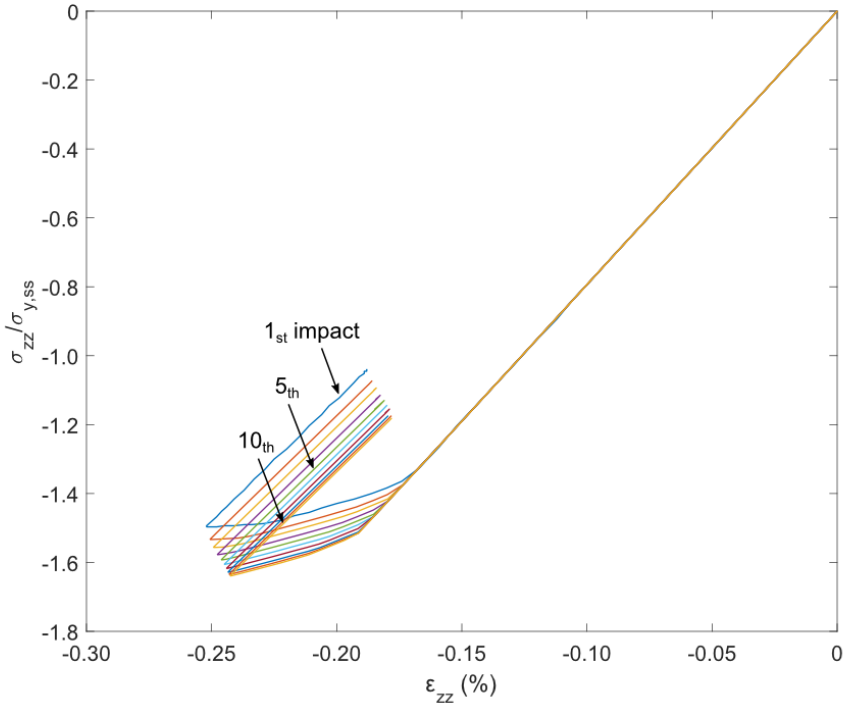

Figure 7. Normalized mormal stress at z-direction with respect the strain at the trailing edge of the foil profile at fixed end.

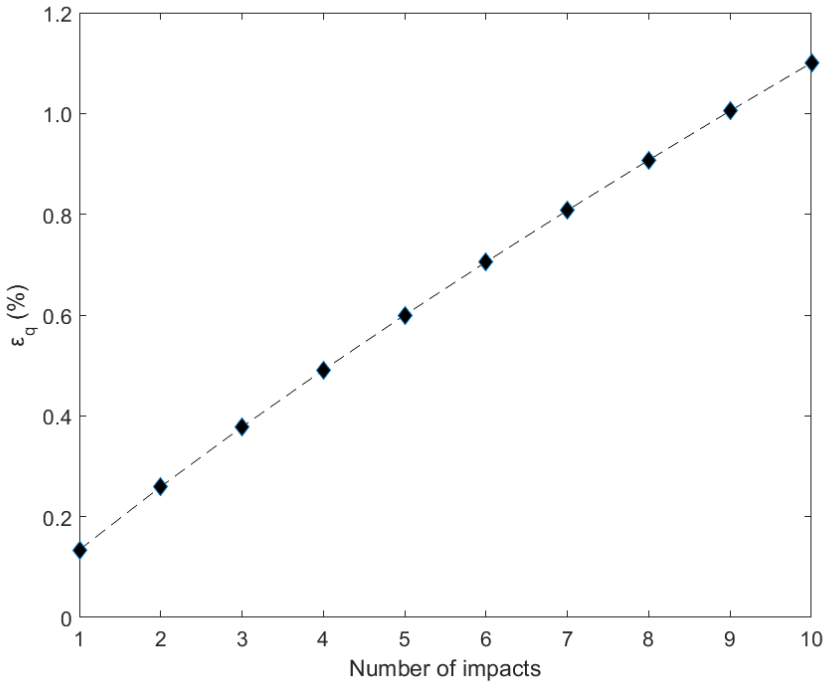

Figure 8. Equivalent plastic strain of the stainless steel material of the turbine blade, with respect the number of impacts.

4. CONCLUSIONS

Impact from sea animals becomes an important loading case on tidal turbines, due to the increase of offshore tidal turbine devices installation. In the present work, a full-scale tidal turbine blade was modelled, investigating its dynamic response under impact loading with killer whale. Stainless steel material was considered for the tidal turbine blade, attempting to evaluate its impact resistance, compared with carbon steel, which is most commonly used. The blade was assumed fixed at the center of the rotor, while velocity was applied to the killer whale. The velocity of the sea animal (v_1) was adopted accordingly, in order to have similar initial kinetic energy on the model, such as in a real case scenario during the operation conditions of a full-scale tidal turbine. Considering velocity of the sea animal equal to v_1, the turbine blade deforms elastically. However, applying velocities higher than two times of v_1, plastic deformation of the blade was observed. It is also important to note that the blade deflects on x-direction, which corresponds to the velocity of the killer whale, and also on y-direction due to the twist of the foil profiles along the turbine blade. Considering this observation, two dimensional velocity of the whale might affect the plastic deformation of the blade and it is an open issue for further investigation. Furthermore, the dynamic response and the accumulation of plastic deformation in the stainless steel material of the blade was compared with a blade made of carbon steel, for different velocities of the killer whale. Assuming AISI 1020 carbon steel material, the blade deformed plastically in higher velocities of the sea animal, compared with the case of stainless steel material of Grade 304. Therefore, the values of equivalent plastic are lower for the carbon steel material strain in the same

range of velocities of the killer whale. However, the stainless steel material constitutes a promising material for such a device, considering the reduced maintenance costs and the elastic deformation of the blade for the assumed operational conditions; the blade deforms plastically in a significantly higher sea animal velocity. Finally, in case of multiple impacts, the material of the turbine blade hardens leading to reducing the plastic strain rate increase. Simulating ten impacts, the equivalent plastic strain in the turbine blade's material is slightly higher than 1%, concluding that the turbine blade is well before its ultimate strength. However, the accumulation of plastic strain in the blade due to multiple impacts and the damage of the material is an open issue for further examination.

ACKNOWLEDGEMENT

The research work is sponsored by Centre for Advanced Materials for Renewable Energy Generation, EPSRC (Grant Ref: EP/P007805/1).

REFERENCES

Abbott, I. H., & Von Doenhoff, A. E. (1959). *Theory of wing sections.* New York: Dover Publications.

Asserin, J., Zahouani, H., Humbert, P., Couturaud, V., & Mougin, D. (2000). Measurement of the friction coefficient of the human skin in vivo: quantification of the cutaneous smoothness. *Colloids and surfaces B: Biointerfaces, 19*(1), 1-12.

Bahaj, A. S., Batten, W. M., & McCann, G. (2007a). Experimental verifications of numerical predictions for the hydrodynamic performance of horizontal axis marine current turbines. *Renewable energy, 32*(15), 2479-2490.

Bahaj, A. S., Molland, A. F., Chaplin, J. R., & Batten, W. M. (2007b). Power and thrust measurements of marine current turbines under various hydrodynamic flow conditions in a cavitation tunnel and a towing tank. *Renewable energy, 32*(3), 407-426.

Barnsley, M. J., & Wellicome, J. F. (1992). Wind tunnel investigation of stall aerodynamics for a 1.0 m horizontal axis rotor. *Journal of Wind Engineering and Industrial Aerodynamics, 39*(1-3), 11-21.

Bashistakumar, M., & Pushkal, B. (2018). Finite element analysis of orthogonal cutting forces in machining AISI 1020 steel by using a carbide tip tool. *Journal of Engineering Sciences, 5*(2), A1-A10.

Batten, W. M., Bahaj, A. S., Molland, A. F., & Chaplin, J. R. (2006). Hydrodynamics of marine current turbines. *Renewable energy, 31*(2), 249-256.

Campbell-Malone, R. P. (2007). *Biomechanics of North Atlantic right whale bone: mandibular fracture as a fatal endpoint for blunt vessel-whale collision modeling.* PhD diss., Massachusetts Institute of Technology.

Carlson, T. J., Elster, J. L., Jones, M. E., Watson, B. E., Copping, A. E., Watkins, M. L., Jepsen, R. A., & Metzinger, K. (2012). *Assessment of strike of adult killer whales by an OpenHydro tidal turbine blade.* Pacific Northwest National Lab. (PNNL), Richland, WA (United States).

Commission of the European Communities, DGXII (1996). *Wave Energy Project Results: The exploitation of tidal marine currents.* Report EUR16683EN.

Dassault Systèmes. (2015). *SolidWorks.* Retrieved from https://www.3ds.com/products-services/solidworks/

Day, A., Babarit, A., Fontaine, A., He, Y. P., Kraskowski, M., Murai, M., Penesis, I., Salvatore, F., & Shin, H.K. (2015). Hydrodynamic modelling of marine renewable energy devices: A state of the art review. *Ocean Engineering, 108*, 46-69.

Douglas, C. A., Harrison, G. P., & Chick, J. P. (2008). Life cycle assessment of the Seagen marine current turbine. *Proceedings of the Institution of Mechanical Engineers, Part M: Journal of Engineering for the Maritime Environment, 222*(1), 1-12.

Ellis, R., Allmark, M., O'Doherty, T., Mason-Jones, A., Ordonez-Sanchez, S., Johannesen, K., & Johnstone, C. (2018). Design process for a scale horizontal axis tidal turbine blade. *Proceedings of the 4th Asian Wave and Tidal Energy Conference.*

Fraenkel, P. L. (2002). Power from marine currents. *Proceedings of the Institution of Mechanical Engineers, Part A: Journal of Power and Energy, 216*(1), 1-14.

Funke, S. W., Farrell, P. E., & Piggott, M. D. (2014). Tidal turbine array optimisation using the adjoint approach. *Renewable Energy, 63*, 658-673.

Grear, M. E. (2018). *Characterization of Marine Mammal Biomechanics to Evaluate Tidal Turbine Collision Impact.* PhD diss., University of Washington.

Grear, M. E., & Motley, M. R. (2015). Numerical Modeling of the Impact Response of Tidal Devices and Marine Mammals. *Proceedings of the 11th European Wave and Tidal Energy Conference.* Nantes, France.

Hepperle, M. (2011). *JAVAFOIL user's guide.* Retrieved January 2021, from www.mh-aerotools.de/airfoils/java/JavaFoil%20Users%20Guide.pdf

Hibbitt, H., Karlsson, B., & Sorensen, P. (2016). Abaqus analysis user's manual version 2016. *Dassault Systèmes Simulia Corp, Providence, RI*.

Johnson, G. R., & Cook, W. H. (1985). Fracture characteristics of three metals subjected to various strains, strain rates, temperatures and pressures. *Engineering fracture mechanics, 21*(1), 31-48.

Lee, S., Barthelat, F., Hutchinson, J. W., & Espinosa, H. D. (2006). Dynamic failure of metallic pyramidal truss core materials–Experiments and modeling. *International Journal of Plasticity, 22*(11), 2118-2145.

Ogden, R. W. (1972). Large deformation isotropic elasticity–on the correlation of theory and experiment for incompressible rubberlike solids. *Proceedings of the Royal Society of London. A. Mathematical and Physical Sciences, 326*(1567), 565-584.

Olczak, A., Stallard, T., Feng, T., & Stansby, P. K. (2016). Comparison of a RANS blade element model for tidal turbine arrays with laboratory scale measurements of wake velocity and rotor thrust. *Journal of Fluids and Structures, 64*, 87-106.

Payne, G. S., Stallard, T., & Martinez, R. (2015). Experimental Investigation of Tidal Rotor Loading due to Wave, Current and Impact with Sea Animals. *Proceedings of the 11th European Wave and Tidal Energy Conference.* Nantes, France.

Payne, G. S., Stallard, T., & Martinez, R. (2017). Design and manufacture of a bed supported tidal turbine model for blade and shaft load measurement in turbulent flow and waves. *Renewable Energy, 107*, 312-326.

Shiekh Elsouk, M. N., Santa Cruz, A., & Guillou, S. (2018). Review on the characterization and selection of the advanced materials for tidal turbine blades. *Proceedings of the 7th International Conference on Ocean Energy.* Cherbourg, France.

Stallard, T., Collings, R., Feng, T., & Whelan, J. (2013). Interactions between tidal turbine wakes: experimental study of a group of three-bladed rotors. *Philosophical Transactions of the Royal Society A: Mathematical, Physical and Engineering Sciences, 371*(1985), 20120159.

Whelan, J. I., & Stallard, T. (2011). Arguments for modifying the geometry of a scale model rotor. *Proceedings of 9th European Wave and Tidal Energy Conference (EWTEC2011).* Southampton, UK.

Yeoh, O. H. (1993). Some forms of the strain energy function for rubber. *Rubber Chemistry and technology, 66*(5), 754-771.